Journal of Materials Chemistry A

Accepted Manuscript

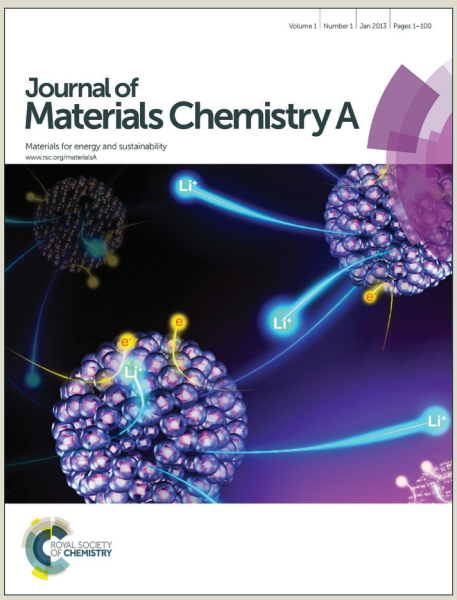

This is an *Accepted Manuscript*, which has been through the Royal Society of Chemistry peer review process and has been accepted for publication.

Accepted Manuscripts are published online shortly after acceptance, before technical editing, formatting and proof reading. Using this free service, authors can make their results available to the community, in citable form, before we publish the edited article. We will replace this *Accepted Manuscript* with the edited and formatted *Advance Article* as soon as it is available.

You can find more information about *Accepted Manuscripts* in the Information for Authors.

Please note that technical editing may introduce minor changes to the text and/or graphics, which may alter content. The journal's standard Terms & Conditions and the Ethical guidelines still apply. In no event shall the Royal Society of Chemistry be held responsible for any errors or omissions in this *Accepted Manuscript* or any consequences arising from the use of any information it contains.

ROYAL SOCIETY OF CHEMISTRY

www.rsc.org/materialsA

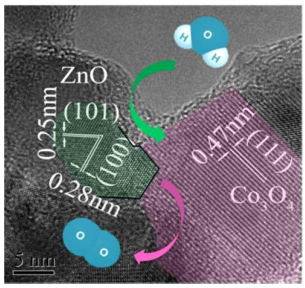

ZnO and Co_3O_4 in the interface of zinc-cobalt oxides work in a cooperative way as water adsorption site and water oxidation site, respectively.

Journal of Materials Chemistry A Accepted Manuscript

Journal of Materials Chemistry A

Cite this: DOI: 10.1039/c0xx00000x

www.rsc.org/xxxxxx

PAPER

Zinc-cobalt oxides as efficient water oxidation catalysts: the promotion effect of ZnO

Feng Rong,[a,b] Jiao Zhao,[a] Panpan Su,[a,b] Yi Yao,[a,b] Mingrun Li, [a] Qihua Yang,*[a] Can Li*[a]

Received (in XXX, XXX) Xth XXXXXXXXX 20XX, Accepted Xth XXXXXXXXX 20XX

DOI: 10.1039/b000000x

Herein, we report the promotion effect of ZnO in water oxidation catalyzed by Co_3O_4. Zinc-cobalt oxides—$ZnCo_xO_y$ were prepared via calcination of Zn-Co_x-coordination polymers. The results of XRD, Co K-edge XANES and EXAFS show that Co/Zn ratio greatly affected the oxidation state of Co and local structure of $ZnCo_xO_y$ oxides. With Co/Zn ratio higher than 3.0, Zn (II) prefers to substitute in the lattice of Co_3O_4. The integrated ZnO and Co_3O_4 composites were formed at Co/Zn ratio less than 2.0. The HR-TEM images show that ZnO and Co_3O_4 compactly contact to form the interfaces in the composites. In both the chemical water oxidation and the visible-light-driven photocatalytic water oxidation ($[Ru(bpy)_3]^{2+}$-persulfate system), Zn substituted in the spinel structured Co_3O_4 oxide cannot significantly improve the water oxidation activity and only the integrated ZnO and Co_3O_4 composites afford much higher TOFs than Co_3O_4. This suggests the existence of the cooperation effect between ZnO (water adsorption site) and Co_3O_4 (water oxidation site). Our results provide a facile approach to design composite catalysts for water oxidation reaction.

Introduction

Producing hydrogen (H_2) fuels and storing the solar energy through water splitting ($2H_2O \rightarrow 2H_2 + O_2$) are efficient strategies for using the renewable but intermittent sunlight.[1-3] The four-electron involved water oxidation for O_2 evolution is one of the biggest challenges for photocatalytic production of solar fuels because this half reaction usually has slower kinetics and needs larger overpotential than the reduction half reaction.[4,5] In the past decades, both homogeneous and heterogeneous catalysts have been developed for enhancing the reaction rate or lowing the overpotential for oxygen evolution reaction (OER). [6-14]

In the early works, the efficient catalysts for OER are generally using noble metals such as Ir and Ru. [11,14-17] Great efforts have been made for replacing noble metals with earth-abundant metals.[10,18] Recent advances show that Ni-, Fe-, Co- and Mn-based metal oxides could be used as efficient catalysts for OER either via electrochemical or photocatalytic approaches.[19-23] For example, mesoporous cobalt oxides and mesoporous silicas supported manganese and cobalt oxides exhibit high activity for OER either using Ce (IV) as oxidant or driven by visible light.[9,24-26] More importantly, Nocera and co-workers reported that a Co-Pi catalyst prepared through an electrodeposition approach acts as efficient electrocatalyst for OER in a neutral aqueous solution.[27]

In nature, PSII is responsible for water oxidation reaction. Studies show that the active site for OER is a $CaMn_4O_5$ complex with three Mn and one Ca forming a distorted $CaMn_3O_4$ cubane and the fourth Mn ion bonded to this cubane by μ–oxido ligands.[28-30] Interestingly, it was found that Ca^{2+} plays a vital role in the performance of $CaMn_4O_5$, though the function of Ca^{2+} is not clearly verified.[31] Inspired by PSII system, calcium-manganese oxides with crystalline or amorphous structure have been used as artifical OER catalysts. Similar to PSII system, Ca^{2+} is also necessary for obtaining higher catalytic activity for calcium-manganese oxides. In addition to Ca^{2+}, the accleration effect of other alkaline-earth metals was clearly observed for manganese oxides in OER, such as Sr.[8] Very recently, Sun and Asefa reported that zinc-substituted cobalt oxides and hydroxides are efficient electrocatalysts in the electrochemical water oxidation and exhibit lower overpotentials than monometallic cobalt-based materials.[32,33] Thus, the doping of some non-active metal to metal oxides for OER is a very important approach for the design of efficient water oxidation catalysts.

Herein, we reported the synthesis of zinc-cobalt oxides—$ZnCo_xO_y$ via calcination of Zn-Co_x-coordination polymers based on "escape by crafty scheme" strategy[34-36] as water oxidation catalysts. The relationship between Co/Zn molar ratio and the water oxidation activity was investigated. It was found that (1) Zn^{2+} ion substituted in the spinel structured Co_3O_4 oxide can not significantly improve the water oxidation activity; (2) The integrated interface between ZnO and Co_3O_4 could efficiently accelerate the oxygen evolution rate in both the chemical water oxidation using Ce(IV) as oxidant and the visible-light-driven photocatalytic water oxidation in $[Ru(bpy)_3]^{2+}$-persulfate system; (3) $ZnCo_xO_y$ oxides synthesized via "escape by crafty scheme" strategy is more active than those prepared with conventional co-precipitation method, probably due to the existence of more interfaces between ZnO and Co_3O_4.

Journal of Materials Chemistry A Accepted Manuscript

Experimental section

Chemicals and materials

All chemicals were used as received unless otherwise stated. 3,4,9,10-Perylenetetracarboxylic dianhydride (PTCDA) was purchased from Alfa Aesar. Zinc acetate dehydrate ($Zn(OAc)_2·2H_2O$) was purchased from Kemiou. Cobalt acetate tetrahydrate ($Co(OAc)_2·4H_2O$), sodium sulfate (Na_2SO_4), sodium persulfate ($Na_2S_2O_8$) and ammonium cerium (IV) nitrate ($(NH_4)_2Ce(NO_3)_6$) were purchased from Sinopharm Chemical Reagent Company. Tris(2,2'-bipyridyl)dichlororuthenium (II) hexhydrate ($Ru(bpy)_3Cl_2·6H_2O$) was purchased from Sigma-Aldrich. Deionized water was used throughout the experiments.

Synthesis of $ZnCo_xO_y$ using Zn-Co_x-coordination polymer

$ZnCo_xO_y$ were synthesized according to our previous report[37] via calcination of Zn-Co based coordination polymers (Zn-Co_x-P) except that the calcination temperature in this work was 380 °C instead of 550 °C.

In a typical synthesis, 12.5 mL of NaOH solution (0.064 M) containing PTCDA (0.2 mmol) was added dropwise to 22.5 mL of aqueous solution containing 0.4 mmol of $Zn(OAc)_2·2H_2O$ and $Co(OAc)_2·4H_2O$. After stirring at room temperature for 30 min, the reaction mixture was transferred into a Teflon-lined stainless steel vessel (45 mL) and heated at 100 °C for 24 h. After cooling down to room temperature, the precipitate was collected by centrifugation and washed several times with water. $ZnCo_xO_y$ oxides were obtained via calcination of Zn-Co_x-P in air at 380 °C for 1 h with a heating rate of 5 °C min^{-1}, where x is Co/Zn molar ratio.

Synthesis of $ZnCo_xO_y$ oxides by co-precipitation method

$Zn(OAc)_2·2H_2O$ and $Co(OAc)_2·4H_2O$ with different Co/Zn molar ratio were dissolved in deionized water, and then sodium oxalate aqueous solution was added dropwise to the mixture solution of metal acetates with stirring. After refluxing for 24 h, the precipitate was collected by filtration, washed with water and dried, and finally calcined in air at 420 °C for 4 h. The obtained samples were denoted as CP-$ZnCo_xO_y$ (x=3.3, 2.2, 1.1 and 0.4), where x is Co/Zn molar ratio.

Characterization

The thermogravimetric (TG) analysis was performed under air atmosphere with a heating rate of 5 °C min^{-1} by using a NETZSCH STA-449F3 thermogravimetric analyzer. The powder X-ray diffraction data (PXRD) were collected on a Rigaku D/Max2500PC diffractometer with Cu Kα radiation (λ=1.5418 Å) over the 2θ range of 15°-70° with a scan speed of 5° min^{-1} at room temperature. Scanning electron microscopy (SEM) was undertaken on a JEOL JSM-6360 scanning electron microscope operating at an acceleration voltage of 20 kV. The samples were sputtered with gold prior to imaging. High-resolution transmission electron microscopy (HR-TEM) images were recorded on a FEI Tecnai F30 microscope with a point resolution of 0.20 nm operated at 300 kV. The metal content was determined by PLASAM-SPEC-II inductively coupled plasma atomic emission spectrometry (ICP). X-ray absorption fine structure (XAFS) experiments were conducted at 1W2B beamline of the Beijing Synchrotron Radiation Facility (BSRF). Samples were ground into fine powers and then smeared on scotch tapes. Co K-edge X-ray adsorption near edge structure (XANES) and extended X-ray absorption fine structure (EXAFS) were collected at room temperature in transmission mode. The storage ring was working at 2.5 GeV with a maximum electron current of about 250 mA. Data were collected using a Si (111) double-crystal monochromator and analyzed using the IFEFFIT program.

Water oxidation using Ce (IV) as oxidant

In a typical reaction, 5 mL of deionized water was placed in a three-necked bottle, followed by the addition of 5 mL $(NH_4)_2Ce(NO_3)_6$ (0.75 M) and 5 mL catalyst suspension (25 mg catalyst was dispersed in 5 mL deionized water). Before stirring, the system was sealed except that one of the necks was connected to a graduated pipette with a plastic tube. A little soap bubble was dropped in the bottom of the graduated pipette. The oxygen evolution was monitored using the soap bubble. For recycling the catalyst, the solid catalyst was isolated from the reaction system by filtration and directly used for the next run after washing with deionized water and drying at 60 °C.

Photocatalytic water oxidation

The photocatalytic oxygen evolution experiment was performed in a Clark electrode system and a reactor-gas chromatography (GC) combination setup. In a typical Clark electrode experiment, aqueous buffer (Na_2SiF_6–$NaHCO_3$, 0.022−0.028 M) with pH value of 5.2-5.3 was first purged with high-purity nitrogen and 2 mL of buffer was placed in the Clark electrode, followed by addition of 2.5 mg catalyst, 2 mg $Ru(bpy)_3Cl_2·6H_2O$, 7.1 mg $Na_2S_2O_8$, and 21.5 mg Na_2SO_4. Before the Clark electrode system was exposed to light, a baseline was recorded for each test to guarantee no oxygen leakage or side reaction. Oxygen evolution was continuously monitored for at least 200 s by the Clark electrode (Hansatech Instruments DW2/2 unit with an S1 electrode) system after exposure to a 300 W Xe research lamp with a 400 nm cutoff filter. In a typical reactor−GC experiment, the reactor (350 mL) was charged with 80 mL of $NaHCO_3$-Na_2SiF_6 buffer aqueous solution (0.028-0.022M, pH=5.2-5.3), $Na_2S_2O_8$ (0.8 mmol), Na_2SO_4 (4 mmol), $Ru(bpy)_3Cl_2$ (0.035 mmol) and catalyst (20 mg). In this system, $Na_2S_2O_8$ was employed as a two-electron oxidant, and $Ru(bpy)_3Cl_2$ as a photosensitizer. The air in reactor was pumping out for 20 min before it was irradiated with a 300 W Xe research lamp (Ushio-CHRMAX LX300) with a 420 nm cutoff filter. The oxygen concentrations in the head space after 10, 30 and 60 min of illumination were quantitatively analyzed by a gas chromatography (Shimadzu GC-8 A, TCD, Ar carrier).

Results and discussion

Synthesis and characterization

Journal of Materials Chemistry A Accepted Manuscript

This journal is © The Royal Society of Chemistry [year]

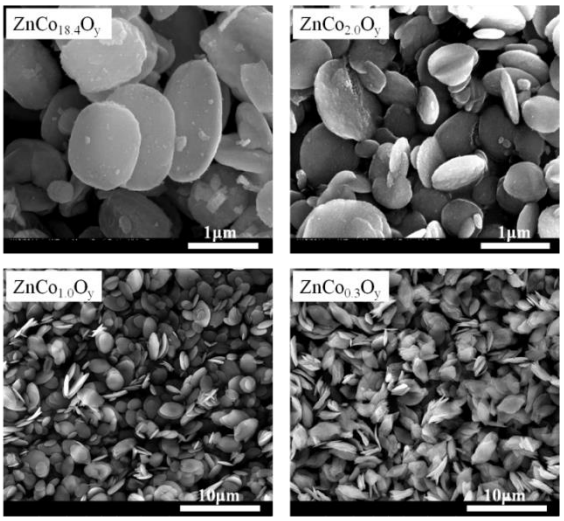

Fig. 1 SEM images of representative $ZnCo_xO_y$ oxides.

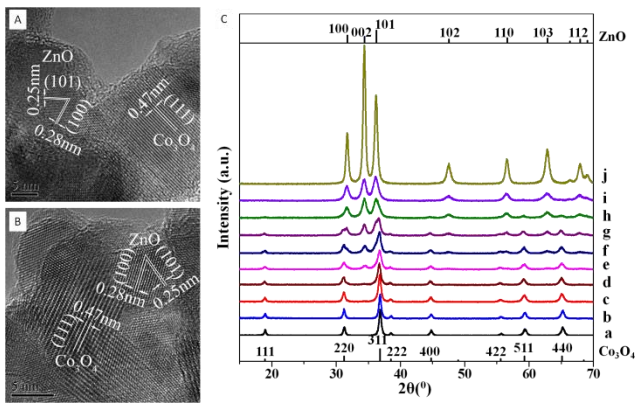

Fig. 2 HR-TEM images of (A) $ZnCo_{1.0}O_y$, (B) $ZnCo_{0.3}O_y$ and (C) XRD patterns of (a) Co_3O_4, (b) $ZnCo_{18.4}O_y$, (c) $ZnCo_{3.9}O_y$, (d) $ZnCo_{3.0}O_y$, (e) $ZnCo_{2.0}O_y$, (f) $ZnCo_{1.5}O_y$, (g) $ZnCo_{1.0}O_y$, (h) $ZnCo_{0.5}O_y$, (i) $ZnCo_{0.3}O_y$, and (j) ZnO; The controlled sample ZnO was prepared as reported previously[37] and the controlled sample Co_3O_4 was prepared in a similar method to $ZnCo_xO_y$ without the addition of $Zn(OAc)_2$ for the synthesis of coordination polymers.

The representative SEM images show that $ZnCo_xO_y$ oxides have similar morphology to the corresponding Zn-Co_x-P coordination polymer precursors but smaller particle size due to the large volume shrinkage after removing the ligands by thermal treatment (Fig. 1, S2 and S3). All $ZnCo_xO_y$ have plate-like morphology but with different size. With decreasing the Co/Zn molar ratio, the round-plate like particles were transformed into uniform rhombus lamella particles with the increasing in the particle size.

The XRD patterns of $ZnCo_xO_y$ oxides are summarized in Fig. 2C. For $ZnCo_xO_y$ oxides with Co/Zn ratio higher than 3.0, the main phase is spinel structured Co_3O_4, suggesting that Zn is mainly incorporated into the Co_3O_4 lattice. The HR-TEM (Fig. S4) of $ZnCo_{3.0}O_y$ also proved the purity of Co_3O_4 phase in the catalyst. The XRD patterns of $ZnCo_xO_y$ oxides with Co/Zn ratio in the range of 2.0 to 0.5 clearly show the co-existence of diffraction peaks from both wurtzite structured ZnO and spinel structured Co_3O_4, indicating the formation of ZnO and Co_3O_4 composites. For $ZnCo_{0.3}O_y$, the main phase is cobalt-substituted wurtzite structured ZnO phase. The result clearly indicates that the zinc-substituted spinel structured Co_3O_4, ZnO-Co_3O_4 composites and cobalt-substituted wurtzite structured ZnO could be formed by varying the Co/Zn ratio in the initial Zn-Co_x-P coordination polymer precursors.

The nanostructure of ZnO-Co_3O_4 composites was further characterized by HR-TEM technique. HR-TEM image shows that $ZnCo_{1.0}O_y$ is composed of intimately integrated nanoplates with particle size of *ca.* 10 nm (Fig. 2A), similar to $ZnCo_xO_y$ oxides prepared via calcination at 550 °C.[37] Analysis of the lattice fringe image of $ZnCo_{1.0}O_y$ is consistent with the (111) plane of spinel Co_3O_4 and (101) and (100) planes of hexagonal wurtzite ZnO. Similar to $ZnCo_{1.0}O_y$, the HR-TEM image of $ZnCo_{0.3}O_y$ shows the co-existence of ZnO and Co_3O_4 (Fig. 2B), although nearly no diffractions for Co_3O_4 phase could be observed in the PXRD pattern of $ZnCo_{0.3}O_y$. This is probably due to the low content of Co_3O_4 phase in $ZnCo_{0.3}O_y$.

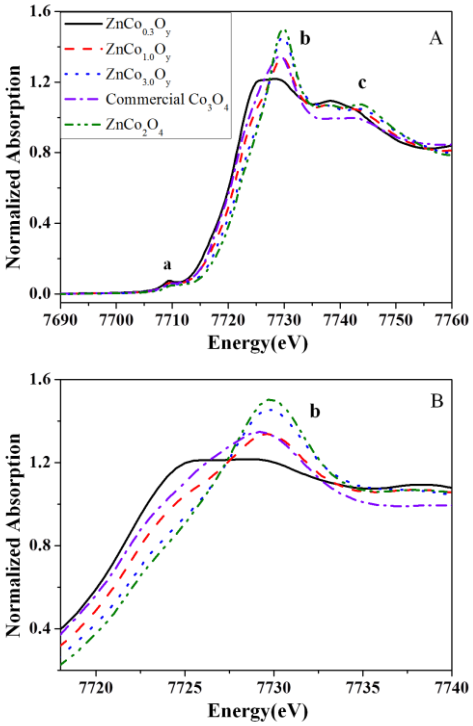

Fig. 3 (A) Co K-edge XANES spectra of commercial Co_3O_4, $ZnCo_2O_4$ synthesized by co-precipitation method and $ZnCo_xO_y$ oxides synthesized using Zn-Co_x-P as precursors and (B) is enlarged part of dominant peak in (A).

The oxidation states of the cobalt ions in the $ZnCo_xO_y$ oxides were investigated by the X-ray absorption near-edge structure (XANES) technique with two standard samples of commercial Co_3O_4 and $ZnCo_2O_4$ synthesized by co-precipitation method for comparison (Fig. 3). Edge-rise energies at the Co K-edge are indicative of the mean oxidation state of Co. According to the method of edge-rise energies,[38] the K-edges increase in the order of $ZnCo_{0.3}O_y$ < commercial Co_3O_4 < $ZnCo_{1.0}O_y$ < $ZnCo_{3.0}O_y$ < $ZnCo_2O_4$, showing that the oxidation state of Co in $ZnCo_xO_y$ oxides follows the same order, which is in agreement with the results of cerimetric titration method[39] (Table 1). A pre-edge step, a dominant peak and a shoulder at post-edge respectively labeled as a, b, and c could be clearly observed in the XANES spectra.

Journal of Materials Chemistry A Accepted Manuscript

The intensity of peak a and also b in XANES are closely related to the symmetry and coordination of the first Co-O coordination.[40] Tetrahedral coordination has a lower intensity peak b than the octahedral one, as well as a higher intensity peak a. Co_3O_4 has spinel crystal structure, with the tetrahedral interstitial sites formed by oxygen packing occupied by Co (II) ion, and the octahedral interstitial sites occupied by Co (III) ion. The intensity of b peak is higher with the increasing of Co valence states in $ZnCo_xO_y$ oxides, because the Zn (II) can only distribute at tetrahedral sites in the spinel Co_3O_4. The Co oxidation state for commercial Co_3O_4 and $ZnCo_2O_4$ is +2.69 and +3, respectively. The b peak of $ZnCo_2O_4$ shifts to higher energy compared with that of commercial Co_3O_4, due to higher Co valence states of $ZnCo_2O_4$. Similarly, the oxidation state of Co ion in $ZnCo_{3.0}O_y$ is higher than that in $ZnCo_{1.0}O_y$. However, $ZnCo_{0.3}O_y$ shows two broad dominant peaks at ~7725.6 eV and ~7729.0 eV. The first dominant peak occurs at similar energy to CoO and the second one is at the same position to Co_3O_4[40], showing that $ZnCo_{0.3}O_y$ has two phases, ZnO with Co (II) substituted in lattice and Co_3O_4.

Table 1. The oxidation state of Co determined by cerimetric titration method.

Sample	Co valence
$ZnCo_2O_4$	+3
Co_3O_4	+2.66
$ZnCo_{18.4}O_y$	+2.82
$ZnCo_{3.9}O_y$	2.86
$ZnCo_{3.0}O_y$	2.88
$ZnCo_{2.0}O_y$	2.87
$ZnCo_{1.5}O_y$	2.82
$ZnCo_{1.0}O_y$	2.73
$ZnCo_{0.5}O_y$	+2.58
$ZnCo_{0.3}O_y$	+2.49

The crystal structures of $ZnCo_xO_y$ oxides were also characterized by extended X-ray absorption fine structure (EXAFS) technique (Fig. 4). Commercial Co_3O_4 affords three peaks located at 1.5 Å, 2.5 Å and 2.9 Å, which could be ascribed respectively to Co-O bond, the next nearest Co-Co and Co-O bonds.[9] $ZnCo_2O_4$ and $ZnCo_xO_y$ ($x \geq 1.0$) show similar EXAFS spectra to commercial Co_3O_4, indicating that cobalt oxide in these samples has spinel structure. Comparing to commercial Co_3O_4, the third peak of $ZnCo_2O_4$ shifts slightly to larger radial distance due to the substitution of Zn (II). All of the peaks of $ZnCo_{3.0}O_y$ match perfectly with those of $ZnCo_2O_4$ even at long radial distances, showing that two samples have the same crystalline structure. This confirms that most of Zn is incorporated into Co_3O_4 lattice for $ZnCo_{3.0}O_y$ as shown by XRD characterization. Except for the first main peak, the positions of the second and third peak of $ZnCo_{1.0}O_y$ shift obviously to larger radial distance, showing the existence of Co-Zn bonds in the next nearest Co-Co and Co-O bonds. This suggests that the local structure of $ZnCo_{1.0}O_y$ is different from both commercial Co_3O_4 and $ZnCo_2O_4$. $ZnCo_{0.3}O_y$ shows radial structure functions similar to Co-doped ZnO,[41-43] implying that most of Co (II) is substituted in the lattice of ZnO, however, the lower radial distance shift of the second peak suggests the formation of spinel Co_3O_4,[40] which is consistent with the HR-TEM results.

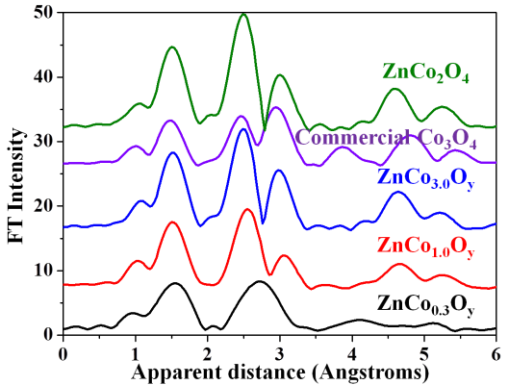

Fig. 4 EXAFS data for commercial Co_3O_4, $ZnCo_2O_4$ and $ZnCo_xO_y$ oxides, the curves are shifted along the y-axis for display purposes.

Water oxidation using $(NH_4)_2Ce(NO_3)_6$ as oxidant

Table 2 The textual parameters and water adsorption capacity of $ZnCo_xO_y$ oxides with different Co/Zn molar ratio and their catalytic activity for water oxidation reactions

Sample	BET surface area (m^2/g)	Water adsorption (mL/cm^2)[a]	TOF*10^3 (mol/molCo·s)[b]	TOF*10^4 (mol/molCo·s)[c]
ZnO	11.6	6.9	0	0
$ZnCo_{0.3}O_y$	37.6	1.6	7.9	3.4
$ZnCo_{0.5}O_y$	33.8	2.1	8.9	2.8
$ZnCo_{1.0}O_y$	32.3	2.2	8.2	2.2
$ZnCo_{1.5}O_y$	29.8	2.0	5.7	1.2
$ZnCo_{2.0}O_y$	35.0	1.8	3.5	1.1
$ZnCo_{3.0}O_y$	30.4	2.1	2.7	1.0
$ZnCo_{3.9}O_y$	27.7	2.3	1.9	0.5
$ZnCo_{18.4}O_y$	25.6	3.3	1.4	0.8
Co_3O_4	27.8	3.2	2.4	0.7

[a] Water adsorption quantity was normalized by the surface area; [b] Water oxidation reaction using Ce (IV) as oxidant. TOFs were claculated in the initial 60 s with assumption that all Co atoms are the active sites; [c] Water oxidation reaction from visible-light-driven in a Clark electrode system. TOFs were claculated in the initial 120 s with assumption that all Co atoms are the active sites.

Chemical water oxidation experiments were performed using $(NH_4)_2Ce(NO_3)_6$ as sacrificial electron acceptor to chemically oxidize water to O_2. Control tests were carried out to verify that no O_2 was produced in the absence of either Ce (IV) or catalyst. We repeated the test at least twice to ensure good reproducibility. ZnO alone cannot catalyze the water oxidation reaction, while Co_3O_4 and $ZnCo_xO_y$ oxides could efficiently catalyze the water oxidation for the production of O_2, suggesting that Co is the active site for water oxidation. The TOFs of $ZnCo_xO_y$ oxides varied in the range of 1.4 x 10^{-3} to 8.9 x 10^{-3} mol/molCo·s depending on the Co/Zn ratio (Table 2). In fact, only surface Co atom could catalyze the water oxidation. For further clarifying the influnce of Co/Zn on the catalytic performance of $ZnCo_xO_y$ oxides, TOF was calculated based on per surface Co atom (Fig. 5). $ZnCo_{0.3}O_y$ with cobalt subsituted into wurtzite structure is more active than Co_3O_4 with TOF of 0.19 mol/mol surface Co·s, suggesting ZnO could promote the activity of Co. Moreover, $ZnCo_xO_y$ composites ($0.5 \leq x < 3.0$) with integrated ZnO and Co_3O_4 are also more active than Co_3O_4, further confirming the promotion effect of ZnO. For $ZnCo_xO_y$ composites ($0.5 \leq x < 3.0$), the TOF increased monotoneously as the Co/Zn molar ratio

Journal of Materials Chemistry A Accepted Manuscript

This journal is © The Royal Society of Chemistry [year]

decreased. $ZnCo_{0.5}O_y$ shows the highest activity among all $ZnCo_xO_y$. This indicates that higher amount of ZnO induces higher activity for $ZnCo_xO_y$ composites ($0.5 \le x < 3.0$). $ZnCo_xO_y$ ($x \ge 3.0$) is less active than $ZnCo_xO_y$ composites ($0.5 \le x < 3.0$) and $ZnCo_{3.9}O_y$ and $ZnCo_{18.4}O_y$ are even less active than Co_3O_4. The characterizations show that Co in $ZnCo_xO_y$ ($x \ge 3.0$) has higher oxidation state than Co_3O_4 and $ZnCo_xO_y$ composites ($0.5 \le x < 3.0$) due to the occupation of Zn(II) at tetrahedral sites in the spinel Co_3O_4. Though the active sites of Co_3O_4 for water oxidation are not very clear at present stage, it could be assumed that they may involve both Co (II) and Co (III). The low activity of $ZnCo_xO_y$ ($x \ge 3.0$) may be due to the combined effect of low content of ZnO and high oxidation state of Co.

The water adsorption experiment suggests that ZnO could adsorb higher amount of water than Co_3O_4. The promotion effect of ZnO may relate with its high water adsorption ability, though no strong relation betweem the activity and water adsorption ability of $ZnCo_xO_y$ composites ($0.5 \le x < 3.0$) could be found. For the generation of promotion effect, ZnO should be close enough to Co active sites. It is reasonable to assume that the interface between ZnO and Co_3O_4 may strongly improve the activity of $ZnCo_xO_y$ oxides in water oxidation reaction.

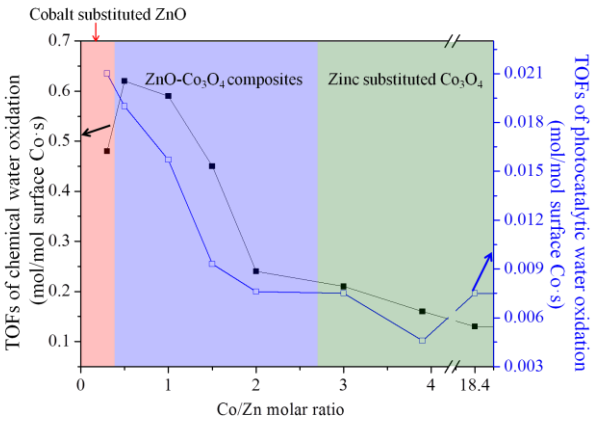

Fig. 5 The influence of Co/Zn ratio on the catalytic performance of $ZnCo_xO_y$ for both chemical and photocatalytic water oxidation (TOF was calculated based on per surface Co atom). It is assumed that $ZnCo_xO_y$ has exposed face of (100) plane, and a simple superposition with the crystal cell of spinel structure and Zn atom is completely identical with Co atom. TOF (mol/mol surface Co·s) = $x*a^2*N_A/(n*m*A*mol\%*t)$, where x = O_2 generated in the initial 60 or 120 s (mol); a = cell parameter (m) of the cubic crystal cell for spinel structure; N_A = Avogadro constant, $6.023*10^{23}$ mol^{-1}; n = number of Co on (100) plane per crystal cell; m = mass of catalyst (g); A = BET surface area (m^2/g); mol% = mole percent of Co of the total mole number of Co and Zn in catalysts ; t = time (s).

A control experiment was also performed for water oxidation using physical mixture of Co_3O_4 and ZnO as catalysts (Co/Zn molar ratio of 1). The physical mixture of Co_3O_4 and ZnO with TOF of 2.3×10^{-3} mol/molCo·s is only slightly more active than Co_3O_4. This result shows that only ZnO closely contacted with Co_3O_4 could show the acceleration effect. For comparison, CP-$ZnCo_xO_y$ oxides with different Co/Zn molar ratios were also prepared using conventional co-precipitation method, which is a general method for the preparation of mixed-metal oxides. All CP-$ZnCo_xO_y$ oxides are composed of irregularly shaped microparticles (Fig. 6A). The XRD results show that CP-$ZnCo_{3.3}O_y$ is Zn (II) substituted spinel Co_3O_4 and CP-$ZnCo_xO_y$ oxides with $x < 3.3$ are composites materials composed with wurtzite structured ZnO and spinel structured Co_3O_4 (Fig. 6B). CP-$ZnCo_{3.3}O_y$ gives the lowest activity among all CP-$ZnCo_xO_y$ oxides (Table 3). For CP-$ZnCo_xO_y$ oxides with $x < 3.3$, the activity increases as the x decreases. This is in a similar tendency to $ZnCo_xO_y$ oxides prepared using coordination polymers as precursors. This result also verifies that the ZnO could greatly enhance the activity of Co for chemical water oxidation reaction. The catalytic activity of CP-$ZnCo_xO_y$ oxides is much lower than $ZnCo_xO_y$ oxides synthesized using coordination polymers as precursor. The possible reason is that the uniform distribution of Zn and Co ions in a well-defined coordination state in the Zn-Co_x-P coordination polymer precursor[36] leads to more interfaces between ZnO and Co_3O_4 in $ZnCo_xO_y$ oxides than that in CP-$ZnCo_xO_y$ oxides synthesis via co-precipitation method.

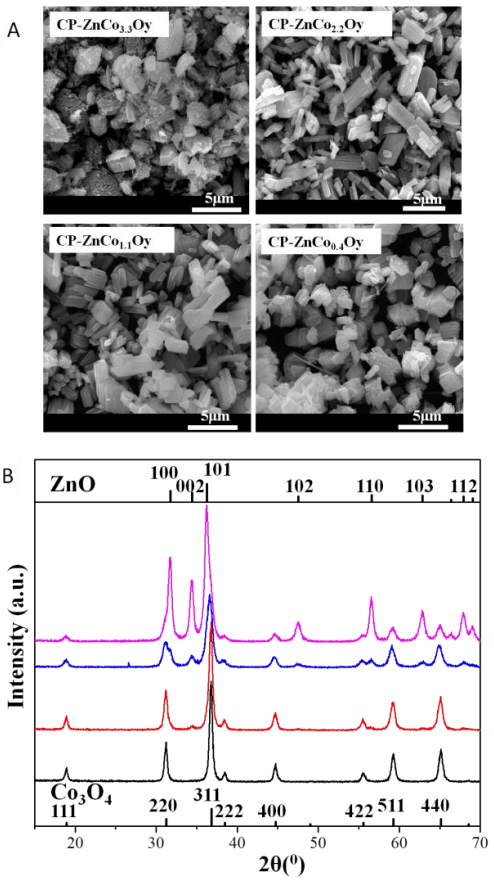

Fig. 6 (A) SEM images and (B) XRD patterns of CP-$ZnCo_{3.3}O_y$, CP-$ZnCo_{2.2}O_y$, CP-$ZnCo_{1.1}O_y$, and CP-$ZnCo_{0.4}O_y$ from bottom to top.

Table 3 The activity of CP-$ZnCo_xO_y$ oxides for water oxidation using Ce (IV) as oxidant

Sample	BET surface area (m^2/g)	TOF*10^3 (mol/molCo·s)[a]	Co/Zn molar ratio[b]
CP-$ZnCo_{3.3}O_y$	25.2	0.4	3.3
CP-$ZnCo_{2.2}O_y$	29.9	0.6	2.2
CP-$ZnCo_{1.1}O_y$	38.2	1.3	1.1
CP-$ZnCo_{0.4}O_y$	28.8	1.0	0.4

[a] TOFs were claculated in the initial 60 s with assumption that all Co atoms are the active sites, [b] Co/Zn molar ratios were measured by ICP.

With $ZnCo_{1.0}O_y$ as model catalyst, the recycle experiment for

Journal of Materials Chemistry A Accepted Manuscript

OER was preformed (Table 4 and Fig. S5). After the reaction, the catalyst was recycled from the reaction solution and used directly for the next run. For the second cycle, the TOF decreases sharply from 8.2×10^{-3} to 2.2×10^{-3} mol/molCo·s. The elemental analysis shows that Co/Zn molar ratio increases from 1.0 to 3.1 after the first cycle, indicating that high acidic reaction medium removes ZnO from $ZnCo_{1.0}O_y$. This was further confirmed by the disappearance of the diffraction peaks assigned to ZnO in the XRD patterns of the recovered catalyst (Fig. S6). The BET surface area increased greatly after the first run due to the removal of ZnO phase. After the first cycle, the activity, Co/Zn ratio and BET surface area are quite stable. This suggests that only ZnO was removed and Zn substituted in Co_3O_4 is stable in acidic medium.

Table 4 The BET surface area, Co/Zn ratio and activity of $ZnCo_{1.0}O_y$ for different cycles in water oxidation using Ce (IV) as oxidant

Cycle	BET surface area (m^2/g)	Co/Zn molar ratio	TOF*10^3 (mol/molCo·s)[a]
2	72.7	3.1:1	2.2
3	73.4	3.2:1	2.5
4	67.9	3.3:1	3.2

[a] TOFs were claculated in the initial 60 s with assumption that all Co atoms are the active sites.

Photocatalytic O_2 evolution

The performance of $ZnCo_xO_y$ oxides was also tested in the photocatalytic water oxidation using $[Ru(bpy)_3]^{2+}$ as visible-light absorber and $S_2O_8^{2-}$ as sacrificial electron acceptor. Control experiments were carried out to verify that no O_2 was produced in the absence of either $[Ru(bpy)_3]^{2+}$ or $S_2O_8^{2-}$ or light or catalyst. The initial photocatalytic water oxidation reaction was performed in a Clark electrode system (Fig. 7A). Because the Clark electrode measures oxygen concentration only in the liquid phase, the total reaction time was set to 200 s, beyond which oxygen evolution goes past the saturation point. We repeated the test at least twice to ensure good reproducibility. The TOFs of $ZnCo_xO_y$ oxides varied in the range of 0.5 to 3.4 $*10^{-4}$ mol/molCo·s assuming that all Co atoms are the active sites (Table 2). As the reaction time increases, the amount of evolved O_2 increases linearly, showing that the catalyst is stable in the initial stage. A TON of 0.08 could be achieved on $ZnCo_{0.3}O_y$ in 200 s, which is almost six times that of Co_3O_4. $ZnCo_xO_y$ ($x \leq 3.9$) is obviously more active than Co_3O_4. We also performed the photocatalytic oxygen evolution in a reactor-gas chromatography (GC) combination system, which allows us to extend the reaction time to 1 h using Co_3O_4, $ZnCo_{3.0}O_y$, $ZnCo_{1.0}O_y$ and $ZnCo_{0.3}O_y$ as catalysts (Fig. 7B). The amount of evolved O_2 increases sharply in initial 10 min. After that, it slows down. A TON of 2.44 could be achieved on $ZnCo_{0.3}O_y$ in 60 min, which is much higher than that of Co_3O_4. Similar to the results in Clark electrode system, $ZnCo_{1.0}O_y$ and $ZnCo_{0.3}O_y$ are more active than Co_3O_4. The above results suggest the promotion effect of ZnO in photocatalytic water oxidation reaction.

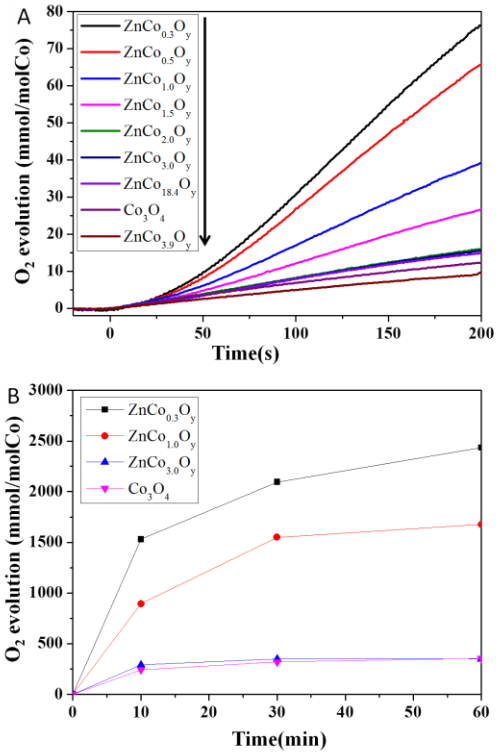

Fig. 7 Oxygen evolution profiles for $ZnCo_xO_y$ oxides utilizing visible-light-driven $[Ru(bpy)_3]^{2+}$-persulfate system, measured by (A) Clark electrode system and (B) gas chromatography system.

As shown in Fig. 5, the TOF of $ZnCo_xO_y$ increases with the decrease in Co/Zn ratio. This is almost the same as that in chemical water oxidation with the exception that $ZnCo_{0.3}O_y$ shows the highest activity instead of $ZnCo_{0.5}O_y$. This result further confirms that ZnO could accelerate the activity of Co in photocatalytic water oxidation reaction. In photocatalytic water oxidation experiments, $[Ru(bpy)_3]^{2+}$ as sensitizer absorbs visible light to generate electro-hole pairs. Following by the sacrificial electron acceptor $S_2O_8^{2-}$ accepts the generated electrons, $[Ru(bpy)_3]^{2+}$ is oxidized to $[Ru(bpy)_3]^{3+}$. After that, $[Ru(bpy)_3]^{3+}$ provides the hole to the oxygen evolution catalyst for finishing the water oxidation reaction. Thus, photocatalytic water oxidation system is more complicated than chemical water oxidation system. In addition to the type of active sites, the interaction of photosensitized with the catalyst, the transfer of sacrificial reagent and the electron and hole could also affect the activity of $ZnCo_xO_y$. The slightly higher activity of $ZnCo_{0.3}O_y$ than $ZnCo_{0.5}O_y$ is probably related with slightly higher surface area of $ZnCo_{0.3}O_y$.

The recycle experiment was also performed using $ZnCo_{1.0}O_y$ as model catalyst utilizing a reactor-gas chromatography (GC) combination system. The obvious decrease in activity was observed for the second cycle (Fig. S7). The XRD characterization of the used catalyst suggests that ZnO is dissolved during the catalytic process (Fig. S8), which probably causes the decrease in activity. The results of both chemical and photocatalytic water oxidation suggest that the interface between ZnO and Co_3O_4 is necessary to improve the activity for water oxidation due to the cooperation between ZnO (non-active site)

Journal of Materials Chemistry A Accepted Manuscript

This journal is © The Royal Society of Chemistry [year]

and Co_3O_4 (water oxidation site).

Conclusion

Using Zn-Co_x-P coordination polymers as precursors, zinc-substituted spinel structured Co_3O_4, ZnO-Co_3O_4 composites and cobalt-substituted wurtzite structured ZnO could be successfully synthesized via a simple thermal treatment. The results of XRD and XAFS experiments suggest that Co/Zn ratio greatly influences the crystal phase and the local Co-O structure of $ZnCo_xO_y$ oxides. With the Co/Zn ratio increasing, main phase transfers from Zn (II) substituted spinel structured Co_3O_4 to co-existence of wurtzite structured ZnO and spinel structured Co_3O_4 and even to Co (II) substituted wurtzite structured ZnO. ZnO-Co_3O_4 composites show much higher activity than Co_3O_4 and zinc-substituted spinel structured Co_3O_4 in both chemical and visible-light driven photocatalytic water oxidation. The present study demonstrates that the promotion effect of ZnO in composite catalysts for water oxidation reaction probably due to the cooperation of ZnO (water adsorption site) and Co_3O_4 (water oxidation site).

Acknowledgements

Funding for this work was provided by NSFC (21325313). The authors would like to acknowledge Zheng Chen for water oxidation test and Yaopeng Zhao for EXAFS measurement

Notes and references

[a] State Key Laboratory of Catalysis, Dalian Institute of Chemical Physics, Chinese Academy of Sciences, 457 Zhongshan Road, Dalian 116023, China

[b] University of Chinese Academy of Sciences, Beijing 100039, China

* To whom correspondence should be addressed.

Email Address: yangqh@dicp.ac.cn; canli@dicp.ac.cn.

Tel: 86-411-84379552; 86-411-84379070.

Fax Number: 86-411-84694447

1. M. Higashi, K. Domen and R. Abe, *J. Am. Chem. Soc.*, 2013, **135**, 10238.
2. T. Minegishi, N. Nishimura, J. Kubota and K. Domen, *Chem. Sci.*, 2013, **4**, 1120.
3. J.H. Yang, D.E. Wang, H.X. Han and C. Li, *Acc. Chem. Res.*, 2013, **46**, 1900.
4. R. Eisenberg and H. B. Gray, *Inorg. Chem.*, 2008, **47**, 1697.
5. J.H. Yang, H.J. Yan, X. Zong, F.Y. Wen, M.Y. Liu and C. Li, *Phil. Trans. Math. Phys. Eng. Sci.*, 2013, **371**, 1996.
6. S. Berardi, G. La Ganga, M. Natali, I. Bazzan, F. Puntoriero, A. Sartorel, F. Scandola, S. Campagna and M. Bonchio, *J. Am. Chem. Soc.*, 2012, **134**, 11104.
7. P.W. Du and R. Eisenberg, *Energy Environ. Sci.*, 2012, **5**, 6012.
8. M. Wiechen, I. Zaharieva, H. Dau and P. Kurz, *Chem. Sci.*, 2012, **3**, 2330.
9. J. Rosen, G. S. Hutchings and F. Jiao, *J. Am. Chem. Soc.*, 2013, **135**, 4516.
10. C. C. L. McCrory, S. Jung, J. C. Peters and T. F. Jaramillo, *J. Am. Chem. Soc.*, 2013, **135**, 16977.
11. J. J. Concepcion, J. W. Jurss, J. L. Templeton and T. J. Meyer, *J. Am. Chem. Soc.*, 2008, **130**, 16462.
12. H. Lv, J. Song, Y. V. Geletii, J. W. Vickers, J. M. Sumliner, D. G. Musaev, P. Koegerler, P. F. Zhuk, J. Bacsa, G. Zhu and C. L. Hill, *J. Am. Chem. Soc.*, 2014, **136**, 9268.
13. M. Zhang, M. de Respinis and H. Frei, *Nat. Chem.*, 2014, **6**, 362.
14. L. L. Duan, F. Bozoglian, S. Mandal, B. Stewart, T. Privalov, A. Llobet and L. C. Sun, *Nat. Chem.*, 2012, **4**, 418.
15. F. A. Frame, T. K. Townsend, R. L. Chamousis, E. M. Sabio, T. Dittrich, N. D. Browning and F. E. Osterloh, *J. Am. Chem. Soc.*, 2011, **133**, 7264.
16. A. Harriman, M. C. Richoux, P. A. Christensen, S. Mosseri and P. Neta, *J. Chem. Soc., Faraday Trans. I*, 1987, **83**, 3001.
17. Y. Jiang, F. Li, F. Huang, B.B. Zhang and L.C. Sun, *Chin. J. Catal.*, 2013, **34**, 1489.
18. M. Gong, Y.G. Li, H.L. Wang, Y.Y. Liang, J. Z. Wu, J.G. Zhou, J. Wang, T. Regier, F. Wei and H.J. Dai, *J. Am. Chem. Soc.*, 2013, **135**, 8452.
19. J. W. Ko, W.-H. Ryu, I.-D. Kim and C. B. Park, *Chem. Commun.*, 2013, **49**, 9725.
20. M. Grzelczak, J. Zhang, J. Pfrommer, J. Hartmann, M. Driess, M. Antonietti and X. Wang, *ACS Catal.*, 2013, **3**, 383.
21. M. M. Najafpour, T. Ehrenberg, M. Wiechen and P. Kurz, *Angew. Chem. Int. Ed.*, 2010, **49**, 2233.
22. P. Liao, J. A. Keith and E. A. Carter, *J. Am. Chem. Soc.*, 2012, **134**, 13296.
23. X. Long, J.K. Li, S. Xiao, K.Y. Yan, Z.L. Wang, H.N. Chen and S.H. Yang, *Angew. Chem. Int. Ed.*, 2014, **53**, 7584.
24. C.-C. Yang, T. M. Eggenhuisen, M. Wolters, A. Agiral, H. Frei, P. E. de Jongh, K. P. de Jong and G. Mul, *ChemCatChem*, 2013, **5**, 550.
25. S. Yusuf and F. Jiao, *ACS Catal.*, 2012, **2**, 2753.
26. F. Jiao and H. Frei, *Chem. Commun.*, 2010, **46**, 2920.
27. M. W. Kanan and D. G. Nocera, *Science*, 2008, **321**, 1072.
28. R. Lomoth, A. Magnuson, M. Sjödin, P. Huang, S. Styring and L. Hammarström, *Photosynth. Res.*, 2006, **87**, 25.
29. W. Lubitz, E. J. Reijerse and J. Messinger, *Energy Environ. Sci.*, 2008, **1**, 15.
30. Y. Umena, K. Kawakami, J.-R. Shen and N. Kamiya, *Nature*, 2011, **473**, 55.
31. M. Miqyass, M. A. Marosvolgyi, Z. Nagel, C. F. Yocum and H. J. van Gorkom, *Biochemistry*, 2008, **47**, 7915.
32. X.X. Zou, A. Goswami and T. Asefa, *J. Am. Chem. Soc.*, 2013, **135**, 17242.
33. X.J. Liu, Z. Chang, L. Luo, T.H. Xu, X.D. Lei, J.F. Liu and X.M. Sun, *Chem. Mater.*, 2014, **26**, 1889.
34. J. Zhao, M.R. Li, J.L. Sun, L.F. Liu, P.P. Su, Q.H. Yang and C. Li, *Chem. Eur. J.*, 2012, **18**, 3163.
35. J. Zhao, P.P. Su, Y.P. Zhao, M.R. Li, Y. Yang, Q.H. Yang and C. Li, *J. Mater. Chem.*, 2012, **22**, 8470.
36. J. Zhao, F.Q. Wang, P.P. Su, M.R. Li, J. Chen, Q.H. Yang and C. Li, *J. Mater. Chem.*, 2012, **22**, 13328.
37. J. Zhao, Y.P. Zhang, P.P. Su, Z.X. Jiang, Q.H. Yang and C. Li, *Rsc Adv.*, 2013, **3**, 4081.
38. H. Dau, P. Liebisch and M. Haumann, *Anal. Bioanal. Chem.*, 2003, **376**, 562.
39. M. Karppinen, M. Matvejeff, K. Salomaki and H. Yamauchi, *J. Mater. Chem.*, 2002, **12**, 1761.
40. T. Liu, H.R. Xu, W. S. Chin, P. Yang, Z.H. Yong and A. T. S. Wee, *J. Phys. Chem.C*, 2008, **112**, 13410.
41. T. Liu, H.R. Xu, W. S. Chin, Z.H. Yong and A. T. S. Wee, *J. Phys.Chem. C*, 2008, **112**, 3489.
42. B.B. Li, Z.F. Chen, F. Boafo, H.L. Shen and J. Luo, *J. Sol-Gel Sci. Technol.*, 2013, **66**, 163.
43. R. Djenadic, G. Akgul, K. Attenkofer and M. Winterer, *J. Phys. Chem. C*, 2010, **114**, 9207.

Journal of Materials Chemistry A Accepted Manuscript